THE ENTRAINMENT OF MASS, MOMENTUM, AND KINETIC ENERGY FROM A TURBULENT BACKGROUND

Oliver R. H. Buxton
Department of Aeronautics
Imperial College London, UK
o.buxton@imperial.ac.uk

Jiangang Chen
Department of Aeronautics
Imperial College London, UK
jiangang.chen@imperial.ac.uk

ABSTRACT

We derive expressions relating the fluxes of momentum and kinetic energy, relative to the mass flux, entrained into a turbulent wake exposed to a turbulent background. These expressions contain correlations between the entrainment velocity and the turbulent fluctuations within the background. We perform high-resolution, simultaneous PIV and PLIF experiments and observe these correlations to be negligible in the far wake such that momentum and kinetic energy are entrained into the wake with the same relative efficiency to mass as from an idealised, non-turbulent background. This is a useful result in the context of modelling since the entrainment hypothesis (Turner, 1986) can still be used to model the entrainment of momentum and kinetic energy. Nevertheless, the entrainment rate of mass is shown to vary spatially, and with the specific nature of the background turbulence, so this in turn drives spatially-varying/background-turbulence-specific entrainment rates of momentum/kinetic energy. Contrastingly, in the near wake, whilst momentum is entrained from a turbulent background with the same relative efficiency to mass as from an idealised non-turbulent background, kinetic energy is entrained more efficiently. This is due to the sum of multiple positive, small-valued correlations between the velocity fluctuations in the background and the entrainment velocity. This also includes entrainment from a non-turbulent background where small correlations are observed between the irrotational background fluctuations and the entrainment velocity. Evidence is also presented that the entrainment velocity scales with the Kolmogorov velocity scale when the background is turbulent.

INTRODUCTION

The spatio-temporal processes by which background fluid is transported and mixed into a turbulent flow are collectively known as entrainment. Entrainment of mass leads to the expansion of the turbulent flow into the background hence it is critical in defining the behaviour of numerous important phenomena ranging from the growth of turbulent boundary layers to meteorological phenomena such as cloud growth/decay. It is governed by small-scale turbulent dynamics within an interfacial layer adjacent to the outermost boundary between the two regions of fluid. In the special case where the background fluid is non-turbulent this layer is known as the turbulent/non-turbulent interface (TNTI). More generally, the background fluid is itself turbulent (e.g. the cloud-containing atmosphere) in which case this layer is known as the turbulent/turbulent interface (TTI).

TNTIs, and entrainment from a non-turbulent background, have been studied for many years. Entrainment is a multi-scale process (Mistry *et al.*, 2016) but in general large-scale processes, in which packets of background fluid are ingested into the flow, are termed engulfment whilst small-scale processes, dominated by viscous diffusion, are termed nibbling. Intermediate length scales are introduced through the contortion of the TNTI into a fractal shape (Sreenivasan & Meneveau, 1986) by turbulent motions within the flow thereby enhancing the surface area over which nibbling occurs. Existing work has shown that in regions of turbulent flows dominated by large-scale coherent motions, e.g. the near field of a turbulent mixing layer, engulfment is active (Yule, 1978) whilst in regions of more "fully-developed" turbulence, e.g. the far field of a jet, engulfment is negligible and nibbling is dominant (Westerweel *et al.*, 2005).

Far less research has been conducted on TTIs and entrainment from a turbulent background. Until recently, zeroth-order questions such as "whether the presence of background turbulence enhances or diminishes entrainment rate in comparison to a non-turbulent background?", and "whether TTIs even exist in scenarios in which the turbulence intensity of the background and primary flow are similar (da Silva *et al.*, 2014)?" remained unanswered. The existence of TTIs, even in scenarios in which the background turbulence intensity is greater than in the primary flow, has now been verified (Kankanwadi & Buxton, 2020). A turbulent background has also now been shown to suppress entrainment rate, with respect to a non-turbulent background, in the far field of a turbulent wake (where nibbling is the dominant entrainment mechanism) (Kankanwadi & Buxton, 2020) and to enhance the entrainment rate in the near field (where engulfment is a significant, if not the dominant, entrainment mechanism) (Kankanwadi & Buxton, 2023). The physics of TTIs have also been shown to be different to those for TNTIs. As first postulated by Corrsin & Kistler (1955), and subsequently verified many years later (Holzner *et al.*, 2007), the physics at the outermost surface of a TNTI are dominated by viscous diffusion, whilst in the inner portion of the TNTI (the so-called turbulent buffer layer (Van Reeuwijk & Holzner, 2013)) they are dominated by inertial vorticity stretching. Contrastingly, in a TTI viscous diffusion is negligible throughout the TTI with vorticity stretching being responsible for producing the discontinuity in enstrophy/vorticity magnitude (Kankanwadi & Buxton, 2022) characteristic of a TTI (Kankanwadi & Buxton, 2020). Studies have also shown that the presence of background turbulence makes the TTI more convoluted than a TNTI (Kankanwadi & Buxton, 2020; Kohan & Gaskin, 2022; Chen & Buxton, 2023).

The above work has focused on the entrainment of mass from the background, whether turbulent or not, but other quantities such as enthalpy, scalar, buoyancy etc. can also be entrained across a TNTI/TTI. In this paper we focus on the entrainment of momentum, in particular the (dominant) streamwise component of momentum, and kinetic energy from a turbulent background. Entrainment of momentum, when considering a suitable control volume encompassing a wake-generating body, is closely related to the drag whilst the entrainment of kinetic energy from geostrophic wind into the atmospheric boundary layer, for example, is important in meteorological phenomena. In the subsequent section we consider the relative "efficiencies" of the entrainment fluxes of momentum and kinetic energy relative to the mass flux for a wake exposed to a turbulent background.

THEORETICAL BASIS

Let us consider a planar wake exposed to both a turbulent and non-turbulent background. In particular, we interrogate a portion of the TTI/TNTI within a plane over a streamwise extent of L_x. We introduce a local coordinate system (ξ_s, ξ_n) which defines the interface-tangential and interface-normal directions, respectively, such that the outermost boundary of the interface (the irrotational boundary for the TNTI) is defined as $\xi_n = 0$. Having done so we can now define the entrainment fluxes of mass $\dot{M}$, the streamwise component of momentum $\dot{P}_x$, and kinetic energy $\dot{K}$ for an incompressible fluid by integrating along the temporally-evolving length of the outermost boundary of the TTI/TNTI, $\ell'(t)$, that is captured in the domain of streamwise extent L_x:

$$\dot{M} = \frac{1}{T}\int_0^T \left(\int_{\ell'(t)} \rho v_e(\xi_s)\mathrm{d}\xi_s \right) \mathrm{d}t =: \overline{\int_{\ell'} \rho v_e \mathrm{d}\xi_s} \qquad (1)$$

$$\dot{P}_x = \overline{\int_{\ell'} \rho U v_e \mathrm{d}\xi_s} \qquad (2)$$

$$\dot{K} = \frac{1}{2}\overline{\int_{\ell'} \rho \left(U^2 + V^2\right) v_e \mathrm{d}\xi_s}. \qquad (3)$$

Here, the entrainment velocity v_e is the relative velocity between the outer surface of the TTI/TNTI and the fluid in a direction normal to the tangent of the TTI/TNTI (Holzner & Lüthi, 2011) and $U = U(\xi_n = 0)$ and $V = V(\xi_n = 0)$ are the streamwise and transverse (in standard Cartesian (x, y) directions) components of the velocity at the outermost boundary of the TTI/TNTI.

Let us now consider entrainment of these various quantities from a non-turbulent background with uniform freestream velocity U_∞. Due to the presence of vorticity on the turbulent side of the TNTI, and the irregular shape of the interface, irrotational velocity fluctuations are observed on the non-turbulent side (Holzner *et al.*, 2009). We thus add this irrotational fluctuation to the freestream velocity such that at $\xi_n = 0 : U = U_\infty + \tilde{u}$ and we note that $V = \tilde{v}$ under the mild assumption that the wake is spreading slowly (via entrainment) with respect to U_∞. The entrainment flux of momentum now becomes

$$\dot{P}_x = \rho \overline{\int_{\ell'} (U_\infty + \tilde{u}) v_e \mathrm{d}\xi_s} \approx \rho \ell \langle (U_\infty + \tilde{u}) v_e \rangle \qquad (4)$$

where $\langle \cdot \rangle$ denotes spatio-temporal ensemble averaging along the outermost boundary of the TNTI within the interrogation domain of streamwise extent L_x, and $\ell = \overline{\ell'}$ with ℓ' being the (temporally) fluctuating length of the TNTI over the domain as before. This last approximation arises from the assumption that the instantaneous length of the interface within the interrogation domain ℓ' does not in any way affect $(U_\infty + \tilde{u})v_e$. The credibility of this assumption is tested empirically and reported in the discussion of figure 2. We are now left with

$$\dot{P}_x \approx \rho \ell U_\infty \langle v_e \rangle + \rho \ell \langle \tilde{u} v_e \rangle. \qquad (5)$$

v_e is a turbulent velocity that is known to scale with a viscous velocity scale (Holzner & Lüthi, 2011; Zhou & Vassilicos, 2017) and is hence focused at high wavenumbers. Contrastingly, $\tilde{u}$ is an irrotational fluctuation driven by irrotational strain/pressure fluctuations (Holzner *et al.*, 2009) induced by the contortion of the TNTI. Since the TNTI is fractal, with this fractal geometry focused in the inertial range of scales, these contortions are likely to drive velocity fluctuations focused at lower (inertial) wavenumbers hence we expect the correlation $\langle \tilde{u} v_e \rangle \approx 0$ leaving us with $\dot{P}_x \approx \rho \ell U_\infty \langle v_e \rangle$. Noting that

$$\dot{M} = \rho \overline{\int_{\ell'} v_e \mathrm{d}\xi_s} \approx \rho \ell \langle v_e \rangle \qquad (6)$$

we see that $\dot{P}_x \approx U_\infty \dot{M}$. Similar analysis yields $\dot{K} \approx \frac{1}{2} U_\infty \dot{P}_x \approx \frac{1}{2} U_\infty^2 \dot{M}$, i.e. there is a direct proportionality between the entrainment fluxes of momentum and kinetic energy and that of mass when the background is an idealised non-turbulent flow.

Let us now apply similar analysis to entrainment into a planar wake exposed to a turbulent background with mean freestream velocity of U_∞ such that $U = U(\xi_n = 0) = U_I + u'$ and $V = V(\xi_n = 0) = v'$ again under a similarly mild assumption that the mean wake spreading rate is small. Here, $U_I = \langle U \rangle \approx U_\infty$ is the ensemble-averaged velocity at $\xi_n = 0$, i.e. the outermost boundary of the TTI. Note also that the velocity fluctuations here (u', v') may in general comprise both standard turbulent fluctuations as well as fluctuations caused by the contortion of the TTI, similarly to the irrotational freestream perturbations caused by a TNTI, although this is a minor detail. The entrained turbulent momentum flux is given by

$$\dot{P}_x = \rho \overline{\int_{\ell'} (U_I + u') v_e \mathrm{d}\xi_s} \approx \rho \ell U_I \langle v_e \rangle + \rho \ell \langle u' v_e \rangle \qquad (7)$$

under the same assumptions as before. We note that for different "flavours" of background turbulence, as parameterised by $\{\mathscr{L}, k\}$, where $\mathscr{L}$ is the integral length scale and k is the turbulence intensity of the background turbulence, the tortuosity of a TTI has been shown to be $\tau = \ell / L_x = \tau(\mathscr{L}, k)$ (Kankanwadi & Buxton, 2020; Kohan & Gaskin, 2022). Nevertheless, when considering a particular "flavour", i.e. fixed $\{\mathscr{L}, k\}$, we still assume ℓ' to have little effect on v_e and $u' v_e$; an assumption that is subsequently empirically tested. This leaves us with

$$\dot{P}_x \approx U_I \dot{M} + \rho \ell \langle u' v_e \rangle. \tag{8}$$

We thus observe that the correlation $\langle u' v_e \rangle$ determines the relative "efficiency" of the entrainment of momentum to the entrainment of mass. When $\langle u' v_e \rangle = 0$ then the relative efficiency for the entrainment of momentum to mass is identical across a TTI to that across an idealised TNTI, with a direct proportionality between $\dot{P}_x$ and $\dot{M}$. Note, however, that the presence of background turbulence is shown to affect entrainment, i.e. $\dot{M} = \dot{M}(\mathscr{L}, k)$ (Kankanwadi & Buxton, 2020, 2023) which will therefore affect the entrainment rate of momentum itself if not the relative efficiency of the entrainment of momentum to mass. Conversely, in a turbulent background when $\langle u' v_e \rangle \neq 0$ this direct proportionality between $\dot{P}_x$ and $\dot{M}$ is broken; when $\langle u' v_e \rangle > 0$ momentum is entrained more efficiently than mass and for $\langle u' v_e \rangle < 0$ it is entrained less efficiently than mass, relative to an idealised non-turbulent background. Note that $v_e > 0$ is defined to be entrainment and $v_e < 0$ to be detrainment (mass ejected from the wake into the background).

We may perform similar analysis for the entrainment of kinetic energy, again making the mild assumption that $V = v'$ since the wake is spreading slowly and a similar assumption relating to ℓ' not affecting v_e or the correlation between v_e and fluctuating velocity components u' and v':

$$\dot{K} = \frac{\rho}{2} \overline{\int_{\ell'} \left[(U_I + u')^2 + v'^2 \right] v_e \mathrm{d}\xi_s} \tag{9}$$

$$\approx \frac{\rho \ell}{2} \left(U_I^2 \langle v_e \rangle + 2U_I \langle u' v_e \rangle + \langle u'^2 v_e \rangle + \langle v'^2 v_e \rangle \right) \tag{10}$$

$$= \frac{1}{2} U_I^2 \dot{M} + \frac{\rho \ell}{2} \left[2U_I \langle u' v_e \rangle + \langle u'^2 v_e \rangle + \langle v'^2 v_e \rangle \right]. \tag{11}$$

As previously, we notice that the correlations appearing in the square brackets of (11) determine whether kinetic energy is entrained more or less "efficiently" than mass, relative to an idealised non-turbulent background. Further, should $\langle u' v_e \rangle \neq 0$ then comparison of (8) and (11) shows that the relative efficiency of the entrainment of kinetic energy to momentum is also broken (with respect to this efficiency across an idealised TNTI) by the presence of background turbulence.

METHODOLOGIES

The experimental configuration was similar to that of Chen & Buxton (2023) in which a circular cylinder of diameter $D = 10$ mm was exposed to various "flavours"/cases of grid-generated background turbulence. The cylinder and the grid were mounted in a hydrodynamics flume and the water depth was set such that the flow's cross section was 0.6×0.6 m^2. The water speed was $U_\infty = 0.38$ m s^{-1} hence the Reynolds number based off the cylinder diameter was $Re_D \approx 3.8 \times 10^3$. Both the length scale $\mathscr{L}$ and intensity k of the background turbulence were independently varied, where $\mathscr{L} \equiv \int_0^{r_0} R_{12}(r) \mathrm{d}r$ in which $R_{12}(r)$ is the correlation between $u'(x,y)$ and $u'(x, y+r)$ integrated to the first zero crossing r_0, and $k \equiv \sqrt{\overline{(u'^2 + v'^2)/2}} / U_\infty$; based off our two-dimensional velocity data. This was achieved by using a combination of regular, and fractal turbulence-generating grids and altering the grid - cylinder streamwise separation. Figure 1(a) outlines the parametric envelope of this campaign at the equivalent position of $x/D = 20$ but in the absence of the cylinder. Runs are split into three groups based on the background turbulence intensity k; group 1 are most similar to the no-grid case whereas $k > k_{wake}$ for group 3.

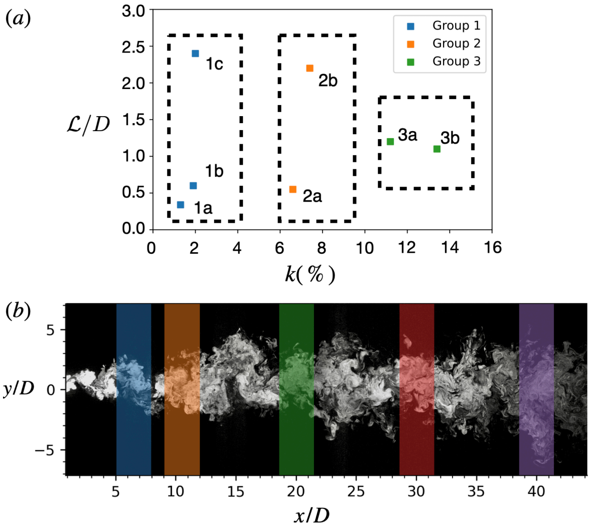

Figure 1. (a) Envelope of background turbulence parameter space $\{\mathscr{L}, k\}$ for the various test cases. (b) Locations of the measurement stations, centred on $x/D = (6.5, 10, 20, 30, 40)$ superimposed on a PLIF image (from (Chen & Buxton, 2023)) illustrating the development of the wake exposed to case 2a background turbulence. The strip colours correspond to the symbols in figures 2 and 3.

Simultaneous, particle image velocimetry (PIV) and planar laser induced fluorescence experiments (PLIF) were conducted. We measured the entrainment fluxes of mass, momentum, and kinetic energy at five different measurement stations centred on $x/D = (6.5, 10, 20, 30, 40)$ downstream of the rear face of the cylinder. Each measurement station had a fixed streamwise extent $L_x = 3D$. Results from our previous work indicate that near-wake effects are particularly important for $x/D \lesssim 15$ (Chen & Buxton, 2023). These measurement stations encompass the near wake ($x/D = (6.5, 10)$), where engulfment is expected to be significant, and the far wake ($x/D = (30, 40)$) where engulfment becomes negligible and nibbling dominates (Westerweel *et al.*, 2005). Their positions are illustrated in figure 1(b).

The presence of both vorticity and turbulent kinetic energy on both sides of a TTI disqualify their use for interface identification. Instead, a high Schmidt number scalar in the form of rhodamine 6G was released from the rear face of the cylinder, ensuring that molecular diffusion occurs over a vanishingly small length scale and hence the scalar acts as a faithful fluid marker. A single hole was used to release the scalar, which was introduced into the flow isokinetically using a Bürket micro dosing unit 7615 connected via a 2 m long cable to the release point, ensuring that the discrete behaviour of the pump was smoothed out. Tests conducted in a non-turbulent background examining the very near field of the wake comparing the extent of the scalar to the enstrophy distribution confirmed that the released scalar was well stirred and faithfully marked the full extent of the wake (Kankanwadi & Buxton, 2020), thereby allowing the PLIF camera to successfully capture the location of the TNTI/TTI. Interface identification was then achieved by using a threshold on the modulus of the captured light intensity gradient, $|\nabla \phi|$. A similar strat-

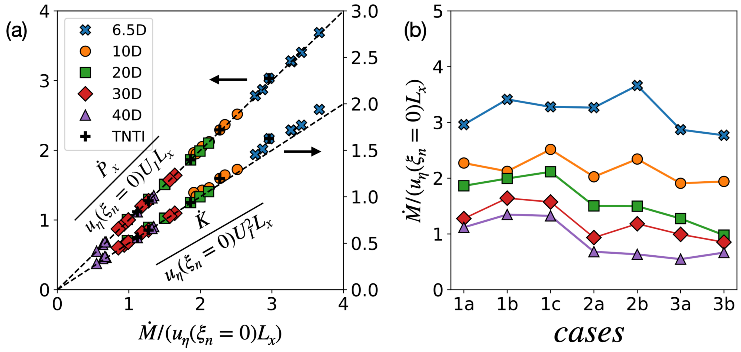

Figure 2. (a) Streamwise momentum entrainment flux $\dot{P}_x$ (top line) and kinetic energy entrainment flux $\dot{K}$ (bottom line) against entrainment mass flux $\dot{M}$. Symbols of the same shape/colour correspond to different cases of background turbulence, as defined in figure 1(a), at the same measurement station. (b) $\dot{M}$ normalised with the local Kolmogorov velocity scale at the outermost boundary of the TNTI/TTI $u_\eta(\xi_n=0)$ for various cases studied. Note subfigure (b) can be cross referenced against subfigure (a) to identify the various cases at the various measurement stations.

egy has been previously shown to work effectively (Kankanwadi & Buxton, 2020). Near Kolmogorov-scale (η) PIV spatial resolution is required to resolve the fine-scale interfacial turbulence; this ranged from 1.7η to 3.2η.

The entrainment mass flux was computed via integrating v_e over the streamwise extent L_x of the PIV field-of-view (Mistry *et al.*, 2016; Kankanwadi & Buxton, 2020), c.f. (1). The approach was modified to include the local streamwise component of the fluid velocity at $\xi_n = 0$ to compute the entrained momentum flux, c.f. (2), and both the streamwise and transverse fluid velocities at $\xi_n = 0$ to compute the entrained kinetic energy flux, c.f. (3). Data was acquired for a period of $T = 25$ s, corresponding to c. 200 periods of vortex shedding, at a measurement frequency of 200 Hz. T corresponds to the averaging-period of (1)–(3). The fixed (in absolute terms) streamwise extent of the field of view, $L_x = 3D$, varied from 147η (case 1a, $x/D = 40$) to 326η (case 3a, $x/D = 6.5$), where η is the Kolmogorov length scale as directly computed along the outermost boundary of the TTI/TNTI (i.e. at $\xi_n = 0$) for the various cases and at the various measurement stations. Alternatively, L_x ranged between 1.25 and 8.8 integral scales of the background turbulence.

RESULTS AND DISCUSSION

The entrained momentum and kinetic energy fluxes are plotted against the entrained mass flux in figure 2(a). The measurements from case 1a, for the non-turbulent background, are denoted with a $+$ sign. We first observe that all entrainment fluxes monotonically diminish with streamwise distance for the non-turbulent background cases. As the turbulent wake approaches the "fully developed" state, the large-scale coherent motions embedded within the wake decay (see figure 1(b)) leaving nibbling as the predominant entrainment mechanism. Assuming that the tortuosity of the TNTI approaches a "fully-developed" state, $\tau \to$ const., then $\ell = \tau L_x \sim L_x$. Similarly, previous work has shown that $v_e \sim u_\eta$ (Holzner & Lüthi, 2011) hence we can deduce $\dot{M} \sim L_x u_\eta$. The similarity in the normalised mass entrainment fluxes in figure 2(b) for case 1a at $x/D = 30$ and $x/D = 40$ attest to this scaling, and give us confidence in our measurements. Further, for the no-grid (TNTI) case 1a, all measurement stations with the exception of one obey the relationships that we previously derived for an idealised non-turbulent background, namely $\dot{P}_x = U_\infty \dot{M}$ and $\dot{K} = \frac{1}{2}\dot{P}_x = \frac{1}{2}U_\infty^2 \dot{M}$. This provides empirical evidence to validate our assumption that ℓ may be taken outside of the spatio-temporal averaging of $\langle (U_\infty + \tilde{u})v_e \rangle$ in (4) and that the correlation $\langle v_e \tilde{u} \rangle \approx 0$. The one exception is the entrained kinetic energy flux at $x/D = 6.5$ which will be discussed subsequently.

We observe the same general trend for a monotonic diminution in the entrainment fluxes with x for the cases with a turbulent background, however the picture is more complicated than for case 1a since, for example, in some cases the entrainment fluxes at $x/D = 40$ are similar to those at $x/D = 20$ for others. Figure 2(b) shows $\dot{M}$ for the various cases studied normalised by $u_\eta(\xi_n = 0)$, the local Kolmogorov velocity scale at the outermost boundary of the TTI/TNTI. In the far wake ($x/D \geq 30$) it can be seen that the entrained mass flux decreases as a function of k (group 3 < group 2 < group 1), confirming the results of (Kankanwadi & Buxton, 2020), whereas in the near wake $\mathscr{L}$ also appears to play a role, with cases 1c and in particular 2b (those with the highest $\mathscr{L}$) seeing enhanced entrainment fluxes.

Importantly, we observe close agreement between the relative efficiencies of the entrainment of momentum/kinetic energy to mass across both TTIs and TNTIs. For all cases and at all measurement stations almost no scatter from the line $\dot{P}_x = U_I \dot{M}$, derived for entrainment from an idealised non-turbulent background, is observed. The picture is similar when considering the relative efficiency of the entrainment of kinetic energy to mass with little scatter from the line $\dot{K} = \frac{1}{2}U_I^2 \dot{M}$ from $x/D \geq 20$. Note, however, that figure 2(b) shows that the presence of background turbulence does affect the mass entrainment rate, which is also spatially developing, i.e. $\dot{M} = \dot{M}(\mathscr{L}, k, x/D)$. Whilst the idealised "efficiency" with which momentum/kinetic energy are entrained with respect to mass is preserved for a turbulent background beyond the near-wake region, our results support the conclusion that the entrainment rate of mass "drives" $\dot{P}_x$ and $\dot{K}$, whose dependencies on $\{\mathscr{L}, k, x/D\}$ are set via $\dot{M}(\mathscr{L}, k, x/D)$. Scatter from the idealised efficiencies is only apparent at the two measurement stations closest to the cylinder, centred on $x/D = (6.5, 10)$, also including the TNTI case 1a. In fact, the entrainment of kinetic energy is shown to be most "efficient" for the TNTI case in the near wake which we discuss subsequently. It is in the near wake that the influence of the energetic coherent motions, evident in figure 1(b), is at its greatest.

(11) dictates that these departures from $\dot{K} = \frac{1}{2}U_I^2 \dot{M}$ be-

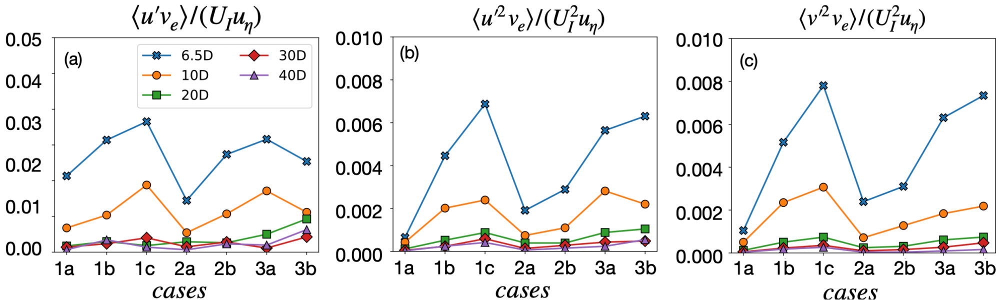

Figure 3. Correlations between the entrainment velocity v_e and fluctuating velocities at the interface location $u', v'(\xi_n = 0)$ from (11). (a) $\langle u'v_e \rangle$, (b) $\langle u'^2 v_e \rangle$, (c) $\langle v'^2 v_e \rangle$.

haviour in the near-wake region require a contribution from correlations between the turbulent velocities u', v' and v_e yet the fact that $\dot{P} \approx U_I \dot{M}$ requires $\langle u'v_e \rangle \approx 0$. Figure 3 shows the spatial evolution of the various correlations of (11) for all cases studied. It can be seen that the correlations are negligible for all measurement stations downstream of $x/D \geq 20$, as expected from figure 2(a). Secondly, even in the near wake the values of these correlations are small. This explains the observation that it is only the entrainment of kinetic energy in the near wake that exhibits an increase in relative efficiency, and not the momentum, as a result of the sum of three small values leading to a noticeable departure from the idealised behaviour. A single contribution from $\langle u'v_e \rangle$ is insufficient for $\dot{P}_x$ to depart from the idealised efficiency. A third general observation is that these correlations are smallest for the group 2 cases, i.e. those with a moderate intensity of the background turbulence, whilst the group 1 and group 3 cases exhibit the largest correlations. A potential explanation is that the fluctuations (u', v') can have a contribution from the underlying turbulence intensity (greatest in group 3) or accelerations/decelerations induced by the "flapping" of the TTI, shown to be less diminished (with respect to the TNTI case 1a) for cases 1b and 1c (Kankanwadi & Buxton, 2023; Chen & Buxton, 2023).

We now explore the nature of the various (weak) correlations in more detail through consideration of the joint probability density functions (JPDFs) between v_e and $(u', \tilde{u}, v')$. Figure 4 shows these JPDFs for the no-grid case and case 3b, which is illustrative of a TTI case, at measurement stations $x/D = (6.5, 10, 20, 40)$. The only JPDFs showing any significant degree of correlation are those at $x/D = 6.5$, reflective of figure 3. For both cases 1a, and 3b and at all measurement stations, the entrainment velocity magnitude is comparable to the velocity fluctuations in the background, whether they be potential (case 1a) or turbulent fluctuations (case 3b). This result for case 1a contradicts our earlier assumption that $\langle \tilde{u} v_e \rangle \approx 0$ due to the fact that there was no overlap in wavenumber space - in fact both velocities $\tilde{u}$ and v_e are focused at high wavenumbers (velocity scales $\sim u_\eta$) but are simply uncorrelated, with the exception of the near wake where they are weakly correlated. For the TTI case 3b the preservation of the extent of the normalised contours of the JPDFs suggests that $v_e \sim u_\eta$. Conversely, for the TNTI case 1a the u_η-normalised velocities diminish in size with downstream distance. At $x/D = 40$ for case 1a, where the flow is the most "fully developed", the contours of the JPDF are approximately bounded by $\pm 5u_\eta$, which is in excellent agreement for the fully-developed oscillating grid TNTI explored by (Holzner & Lüthi, 2011). This shrinking of the normalised contours is suggestive of an alternative scaling for the entrainment velocity other than $v_e \sim u_\eta$ over the streamwise extent of the flow examined, i.e. $x/D < 40$. Over such an extent the turbulence within the wake may not have become "fully developed", and the turbulent Reynolds number remains relatively low. However, another possible explanation is that the $v_e \sim u_\eta$ scaling is broken in the non-equilibrium dissipation paradigm (Zhou & Vassilicos, 2017) in which the dissipation rate is out of equilibrium with the inter-scale flux of turbulent kinetic energy (e.g. Vassilicos, 2015). The scaling $v_e \sim u_\eta$ for TTIs (with an intensely turbulent background, case 3b) is perhaps a result of the fact that background turbulence has the effect of breaking up the coherent motions within the wake more efficiently and a strong contribution from these appears to be a pre-requisite for non-equilibrium dissipation effects (Goto & Vassilicos, 2016). Finally, for both the TNTI case 1a and the TTI case 3b the negative skew for the distribution of v_e reduces with x, explaining the result from figure 2(a) that entrainment fluxes diminish with downstream distance.

CONCLUDING REMARKS

The fact that background turbulence does not substantially alter the relative entrainment efficiencies of kinetic energy/momentum to mass is noted to be a good thing with respect to modelling. In recent years models for entrainment of momentum into wind-farm wakes from the turbulent atmospheric boundary layer (e.g. Luzzatto-Fegiz & Caulfield, 2018) have emerged using the classical entrainment hypothesis $\dot{M} = E\mathscr{V}$ (Turner, 1986) where E is known as the entrainment coefficient and $\mathscr{V}$ is a flow velocity scale used to model the entrainment velocity. These models subsequently proceed to assume that $\dot{P}_x \sim U_\infty \dot{M}$, i.e. the efficiency with which momentum is entrained into the wind-farm wake from a turbulent background is the same as that for the idealised non-turbulent background. Whilst the implications of assuming this efficiency have not previously been discussed, our work is reassuring in the sense that absent of large-scale motions (typical of the near wake in our case) then these assumptions are reasonable. Note, however, that our results are clear that $\dot{M} = \dot{M}(\mathscr{L}, k, x/D)$. Given that the entrainment rate of momentum/kinetic energy is slaved to the mass entrainment rate outside of the near wake, through the idealised efficiency, then it follows that $\dot{P}_x$ and $\dot{K}$ are set by $\dot{M}(\mathscr{L}, k, x/D)$. From a modelling perspective, this requires that $E = E(\mathscr{L}, k, x/D)$ yet figure 2(b) shows that a simple relationship here remains elusive.

We conclude by noting that we have considered a wake in the current work, where the mass entrainment flux drives a transfer of momentum/kinetic energy from a reservoir of high momentum/kinetic energy to low momentum/kinetic energy. For a jet the opposite scenario exists, i.e. the mass entrainment flux drives a transfer of momentum/kinetic energy from a reservoir of low momentum/kinetic energy to high momen-

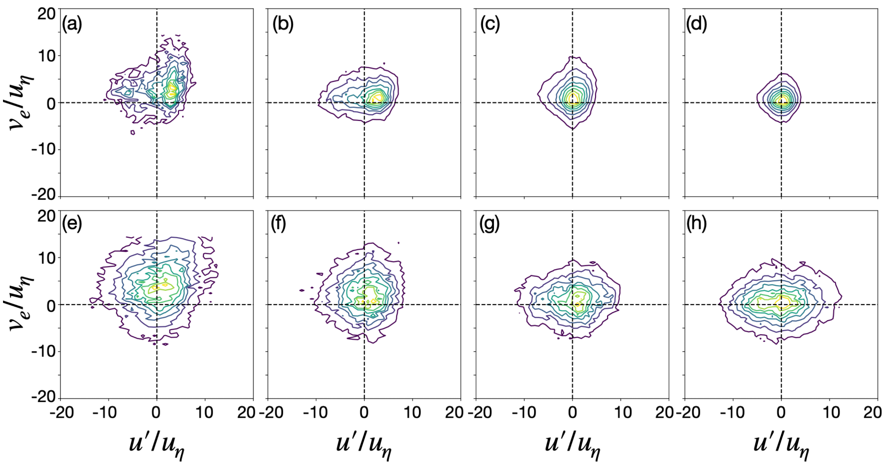

Figure 4. Illustrative joint PDFs between the entrainment velocity v_e and fluctuating velocity at the interface location $u'(\xi_n = 0)$ for case 1a (a TNTI, top row) and case 3b (a TTI, bottom row). (a) and (e) $x/D = 6.5$, (b) and (f) $x/D = 10$, (c) and (g) $x/D = 20$, (d) and (h), $x/D = 40$.

tum/kinetic energy. Nevertheless, our anticipation is that the phenomenology will be qualitatively similar, if slightly quantitatively different. Our previous work has shown astonishingly similar results with regards to the effects of background turbulence on the geometry of TTIs demarcating wakes from a turbulent background (Kankanwadi & Buxton, 2020; Chen & Buxton, 2023) in comparison to those for jets issuing into a turbulent background produced by a random jet array (Kohan & Gaskin, 2022), i.e. non-spatially decaying turbulence. Given the importance of the physics of the TTI in determining the turbulent/turbulent entrainment fluxes (Kankanwadi & Buxton, 2022) we thus postulate similar behaviour in terms of the efficiencies with which momentum and kinetic energy are entrained relative to mass. Further research is, however, required to determine how universal these phenomena are.

[N.B. this paper is an abridged version of Buxton & Chen (2023) published in December 2023.]

REFERENCES

Buxton, O. R. H. & Chen, Jiangang 2023 The relative efficiencies of the entrainment of mass, momentum and kinetic energy from a turbulent background. *Journal of Fluid Mechanics* **977**, R2.

Chen, J. & Buxton, O. R. H. 2023 Spatial evolution of the turbulent/turbulent interface geometry in a cylinder wake. *Journal of Fluid Mechanics* **969**, A4.

Corrsin, S. & Kistler, A. L. 1955 Free-stream boundaries of turbulent flows. *NACA technical report* (1244).

Goto, S. & Vassilicos, J. C. 2016 Unsteady turbulence cascades. *Physical Review E* **94** (5), 053108.

Holzner, M, Liberzon, A, Nikitin, N, Kinzelbach, W & Tsinober, A 2007 Small-scale aspects of flows in proximity of the turbulent/nonturbulent interface. *Physics of Fluids* **19** (7), 071702.

Holzner, M. & Lüthi, B. 2011 Laminar superlayer at the turbulence boundary. *Physical Review Letters* **106** (13), 134503.

Holzner, M., Lüthi, B., Tsinober, A. & Kinzelbach, W. 2009 Acceleration, pressure and related quantities in the proximity of the turbulent/non-turbulent interface. *Journal of Fluid Mechanics* **639**, 153–165.

Kankanwadi, K. S. & Buxton, O. R. H. 2020 Turbulent entrainment into a cylinder wake from a turbulent background. *Journal of Fluid Mechanics* **905**, A35.

Kankanwadi, K. S. & Buxton, O. R. H. 2022 On the physical nature of the turbulent/turbulent interface. *Journal of Fluid Mechanics* **942**, A31.

Kankanwadi, K. S. & Buxton, O. R. H. 2023 Influence of freestream turbulence on the near-field growth of a turbulent cylinder wake: Turbulent entrainment and wake meandering. *Physical Review Fluids* **8** (3), 034603.

Kohan, K. F. & Gaskin, S. J. 2022 On the scalar turbulent/turbulent interface of axisymmetric jets. *Journal of Fluid Mechanics* **950**, A32.

Luzzatto-Fegiz, P. & Caulfield, C-C. P. 2018 Entrainment model for fully-developed wind farms: Effects of atmospheric stability and an ideal limit for wind farm performance. *Physical Review Fluids* **3** (9), 093 802.

Mistry, D., Philip, J., Dawson, J. R. & Marusic, I. 2016 Entrainment at multi-scales across the turbulent/non-turbulent interface in an axisymmetric jet. *Journal of Fluid Mechanics* **802**, 690–725.

da Silva, C. B., Hunt, J. C. R., Eames, I. & Westerweel, J. 2014 Interfacial layers between regions of different turbulence intensity. *Annual Review of Fluid Mechanics* **46** (1), 567–590.

Sreenivasan, K. R. & Meneveau, C. J. F. M. 1986 The fractal facets of turbulence. *Journal of Fluid Mechanics* **173**, 357–386.

Turner, J. S. 1986 Turbulent entrainment: the development of the entrainment assumption, and its application to geophysical flows. *Journal of Fluid Mechanics* **173**, 431–471.

Van Reeuwijk, M. & Holzner, M. 2013 The turbulence boundary of a temporal jet. *Journal of Fluid Mechanics* **739**, 254–275.

Vassilicos, J. C. 2015 Dissipation in turbulent flows. *Annual Review of Fluid Mechanics* **47**, 95–114.

Westerweel, J., Fukushima, C., Pedersen, J. & Hunt, J. C. R. 2005 Mechanics of the turbulent - non-turbulent interface of a jet. *Physical Review Letters* **95** (17), 1–4.

Yule, A. J. 1978 Large-scale structure in the mixing layer of a round jet. *Journal of Fluid Mechanics* **89** (3), 413–432.

Zhou, Y. & Vassilicos, J. C. 2017 Related self-similar statistics of the turbulent/non-turbulent interface and the turbulence dissipation. *Journal of Fluid Mechanics* **821**, 440–457.